Performance of line-scan Raman microscopy for high-throughput chemical imaging of cell population

Ji Qi and Wei-Chuan Shih*

Department of Electrical and Computer Engineering, University of Houston, Houston, Texas 77204, USA

*Corresponding author: wshih@uh.edu

Received 24 December 2013; revised 31 March 2014; accepted 3 April 2014;
posted 3 April 2014 (Doc. ID 203683); published 29 April 2014

We evaluate the performance of line-scan Raman microscopy (LSRM), a versatile label-free technique, for high-throughput chemical imaging of cell population. We provide detailed design and configuration of a home-built LSRM system developed in our laboratory. By exploiting parallel acquisition, the LSRM system achieves a significant throughput advantage over conventional point-scan Raman microscopy by projecting a laser line onto the sample and imaging the Raman scattered light from the entire line using a grating spectrograph and a charge-coupled device (CCD) camera. Two-dimensional chemical maps can be generated by scanning the projected line in the transverse direction. The resolution in the x and y direction has been characterized to be ~600–800 nm for 785 nm laser excitation. Our system enables rapid classification of microparticles with similar shape, size, and refractive index based on their chemical composition. An equivalent imaging throughput of 100 microparticles/s for 1 μm polystyrene beads has been achieved. We demonstrate the application of LSRM to imaging bacterial spores by identifying endogenous calcium dipicolinate. We also demonstrate that LSRM enables the study of intact microalgal cells at the colonial level and the identification of intra- and extracellular chemical constituents and metabolites, such as chlorophyll, carotenoids, lipids, and hydrocarbons. We conclude that LSRM can be an effective and practical tool for obtaining endogenous microscopic chemical and molecular information from cell population.

OCIS codes: (300.6230) Spectroscopy, coherent anti-Stokes Raman scattering; (110.4234) Multispectral and hyperspectral imaging; (350.4855) Optical tweezers or optical manipulation.

http://dx.doi.org/10.1364/AO.53.002881

1. Introduction

Raman scattering provides molecular "fingerprinting" capability due to the inelastic interaction between incident photon and molecular vibration. Using confocal Raman microscopy to study biological cells *in situ* is attractive because molecular information can be obtained without exogenous stains or fluorescence labels [1]. Important examples include the studies of Matthaus *et al.* on the distribution of intracellular substances at different stages of cell mitosis [2]; the identification by Hartsuiker *et al.* and Haka *et al.* of representative constituents in breast cancer [3,4]; time-lapse Raman imaging of a *single* lymphocyte by Pully *et al.* with 2 min temporal resolution [5]; the identification of bacterial strains in biofilms by Beier *et al.* [6]; the study of intracellular delivery and degradation of polymeric nanoparticles by Chernenko *et al.* [7]; the compositional analysis of single microalgal cells [8] by Huang *et al.*; and, the mapping, by Weiss *et al.*, of hydrocarbon deposits in *microalga Botryococcus braunii* [9]. The results from these studies show definitively that the mapping of spatiotemporal chemical composition by Raman spectroscopy can enable important discoveries in biology and biomedicine. However, the small spontaneous Raman scattering cross-section of biological samples, coupled with severe limits on laser power density (~2 mW/μm^2), leads to long pixel imaging times. In general, at least 100 ms of laser dwelling time is needed for a pixel volume of

1559-128X/14/132881-05$15.00/0

~1 μm^3 (1 fL). This limits field size, resolution, and the molecular complexity that can be achieved in spatial chemical maps and the temporal resolution of time-resolved studies. These limitations prevent the acquisition of chemical maps from cell population with optimal spatiotemporal resolution.

A high throughput instrument would enable Raman microscopy to become a viable detection and monitoring tool for analysis at cell population level, which could eventually lead to high-throughput screening techniques. Recent advances in coherent anti-Stokes Raman scattering (CARS) and stimulated Raman scattering (SRS) techniques provide high-speed image acquisition at selected Raman bands, while plasmonics enable surface-enhanced Raman scattering (SERS) when target molecules are adsorbed on Au or Ag nanostructures [10–12]. However, CARS is limited by nonresonant background and spectroscopic interpretation; SRS is not suitable for full-spectrum acquisition; and SERS is a technique only sensitive to surface. In addition to techniques that fundamentally address the intrinsically small Raman scattering cross-section such as the coherent and SERS techniques mentioned above [10–12], an effective solution to the slow mapping speed is through approaches that exploit 2D detector technology to achieve parallel data acquisition. The approach has been used to improve throughput in slit-scan reflectance confocal microscopes [13] and line-scan fluorescence readers for DNA arrays [14]. In Raman spectroscopy domain, a fiber bundle has been employed as a shape-transforming component to relay a 2D scene onto the 1D slit of a spectrograph [15–19]. Free-space approaches have been implemented by Hamada *et al.*, Christensen and Morris [20,21]. Recently, we have implemented a parallel Raman microscopy scheme based on active illumination by a spatial light modulator [22,23]. An excellent study has been performed by Schlucker *et al.* to compare point-scan, line-scan, and global illumination (GI) schemes [24], among which, the line-scan approach provides the highest throughput when full-spectrum Raman images are acquired. GI, in contrast, acquires narrow-and images within each frame and full-spectrum images are accomplished by scanning a bandpass filter. Strictly speaking, GI is not a high-throughput technique because out-of-band Raman photons are not collected at each scanning step. GI might have an advantage when only a small number of Raman bands are needed.

In this paper, we demonstrate that line-scan Raman microscopy (LSRM) can enable rapid classification and counting of hundreds of physically similar organic microparticles, as well as screening hundreds of bacterial spores within a manageable time frame. LSRM also enables the study of living colonial microalgal cells at the *population* and *network* levels and include the identification of intra- and extracellular structural constituents, as well as cell metabolites such as protein, lipids, and hydrocarbons based on their distinct Raman fingerprints.

2. LSRM System Configuration and Characterization

To fully explore the throughput advantage of parallel acquisition, we have employed the 785 nm output of a continuous-wave (cw) titanium:sapphire laser (Spectra-Physics 3900S) pumped by a diode-pumped solid-state 532 nm laser (Spectra-Physics Millennia 10×). As shown in Fig. 1(a), the laser output is transformed by a line-generating optical system consisting of a Powell lens (L1, fan angle 7°, Leading-Tech) and two cylindrical lenses (L2, 100 mm f.l. & L3, 50 mm f.l., Thorlabs) to form a uniform line. This line is relayed to the side-port focal plane of an inverted microscope (Olympus IX70). A dichroic mirror (785 nm RazorEdge dichroic, Semrock) is placed on the beam path to reflect the laser light. A galvanometric mirror (Thorlabs) is employed to scan and de-scan the line in the transverse direction. Epi-Raman is collected by a microscope objective (60× or 10×) and sent through the dichroic mirror and an additional long-wave pass filter (785 nm RazorEdge long pass, Semrock) for laser-intensity reduction and imaged at the entrance slit of a spectrograph with a CCD detector (Princeton LS785).

An essential requirement for high-performance LSRM is intensity uniformity of the excitation laser light along the projected line as well as across the scanning direction. We have evaluated the uniformity in both directions using a polystyrene (PS) plate. Figure 1(b) shows an x–y map (area 100 μm × 100 μm) of the strongest Raman peak, which originates from

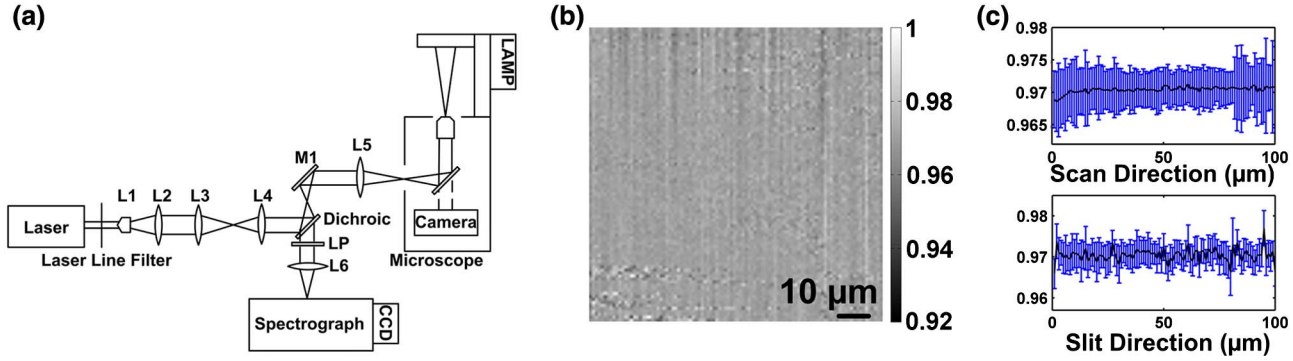

Fig. 1. LSRM system configuration and intensity uniformity: (a) configuration; (b) map of polystyrene (PS) plate; (c) representative intensity profiles along the projected line and scanning directions.

the PS ring breathing mode at 1001 cm^{-1}. The standard deviation of the intensity values is less than 0.4% of the average intensity. To better evaluate the intensity uniformity, Fig. 1(c) displays intensity profiles along the scanning and the line directions. This confirms that the laser power has been evenly distributed along the projected line. The entire laser line was ~120 μm in length, from which the top and bottom 10 μm were not used. Thus the utilization percentage was ~85%. This map could also be used for intensity correction across the field of view. The imaging capability of the microscope has been characterized using PS beads of size from 3 to 500 nm. Figures 2(a) and 2(b) show the maps of 3 and 1 μm PS microparticles generated using the PS peak at 1001 cm^{-1}, respectively. Figure 2(c) shows the Raman map and intensity response in x and y directions of a single 500 nm PS bead. The lateral resolution is estimated to be 600 and 800 nm in x and y directions from the FWHM of the intensity response, respectively. The spectral resolution is better than 5 cm^{-1} according to manufacturer's specifications. The total acquisition time is 2.5 min for an area of 100 μm × 100 μm using a 0.5 μm scanning step size and a 0.75 s dwell time of the projected laser line. In comparison, it would take ~4 h to acquire such a map with similar resolution, step size, and power density using a point-scan system. Assuming that 100% of the area in Fig. 2(b) is packed by 1 μm PS beads, the equivalent imaging throughput is ~100 microparticles/s with 0.5 s laser dwell time and 0.5 μm step size. The power density has been set at ~3 $mW/\mu m^2$ for sample damage threshold considerations. Typically, the x direction resolution is comparable for point-scan and line-scan systems as experimentally observed by Schlucker *et al.* in their comparison of point-scan, line-scan, and GI systems [24]. For line-scan systems, the y direction resolution is slightly worse than that for the x direction, likely due to the lack of confocality along the spectrograph entrance slit, which has been observed by us and Schlucker *et al.* [24].

3. Rapid Counting and Identification of Microparticles

One of the most powerful features of chemical imaging is the ability to classify microparticles of similar size, shape, and refractive index. Although Raman spectroscopy has been a great tool in analytical laboratories for material characterization, its slow imaging speed has prevented the possibility in counting many microparticles rapidly. To evaluate the capability of LSRM, we have prepared samples of mixed 3 μm PS and polymethylmethacrylate (PMMA) microspheres. Figure 3(a) shows the image acquired using a bright-field imaging channel, from which little difference can be observed among these microspheres. LSRM has been performed over a partially overlapping but larger area of the same sample. Images were generated using the PMMA peak at 813 cm^{-1} [Fig. 3(b)] and PS peak at 1001 cm^{-1} [Fig. 3(c)] with the corresponding Raman spectra of these two materials shown in Fig. 3(d). These maps provide unambiguous classification of microspheres of different chemical compositions. Particle counting can be subsequently implemented using thresholding and edge-finding algorithms. The Raman data cube has been collected within 100 s.

4. Rapid Counting and Identification of Bacterial Spores

A natural application for counting and classification of microparticles is bacterial cell analysis [22,23]. Some bacteria are known to "sporulate" to survive harsh environmental conditions. Therefore the study of spores is of great interest in microbiology. In addition, it is critical to detect and analyze spores in biofilms in order to develop optimal treatment strategies in biomedicine. Using *Bacillus subtilis* spore as a model, the bright-field image is shown in Fig. 4(a) over an area of 60 μm × 30 μm. A corresponding Raman map acquired by LSRM using the calcium dipicolinate (CaDPA) Raman band at 1011 cm^{-1} is shown in Fig. 4(b). Figure 4(c) shows the full Raman

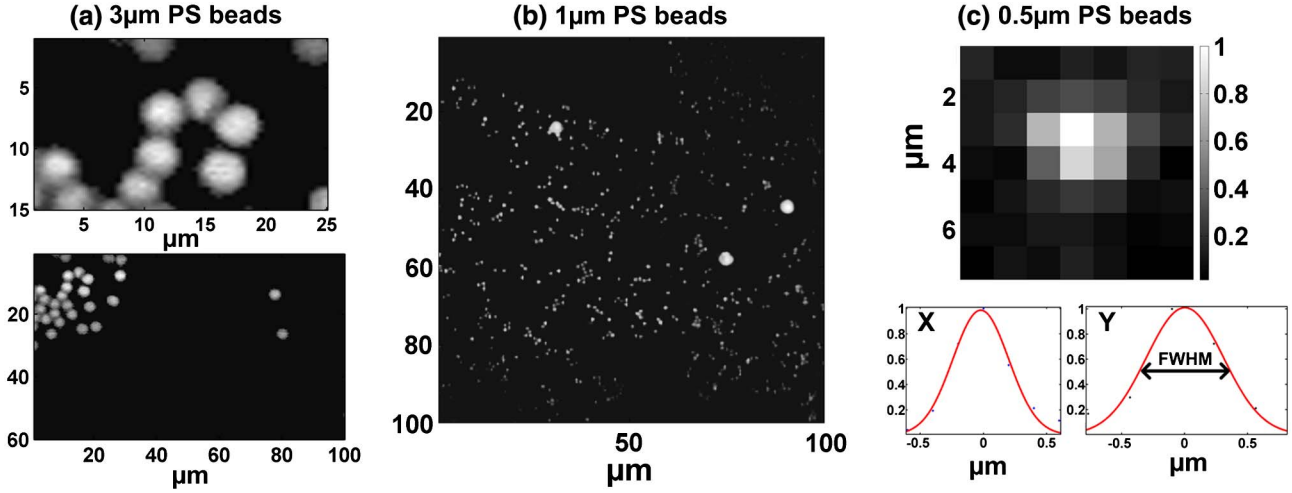

Fig. 2. LSRM system characterization. (a) 3 μm PS beads within a 60 μm × 100 μm area (lower), zoom-in of the upper-left corner (upper). (b) Image of 1 μm PS beads within a 100 μm × 100 μm area (three 3 μm PS beads are included). (c) 500 nm PS bead for estimating the lateral spatial resolution.

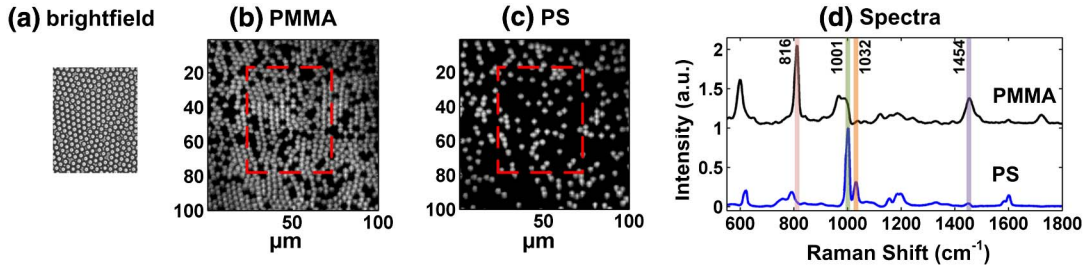

Fig. 3. Rapid identification and counting of microparticles using LSRM. (a) Bright-field image of mixed PS and PMMA microspheres. (b) Map generated using PMMA Raman peak. (c) Map generated using PS Raman peak. (d) Raman spectra of PMMA and PS.

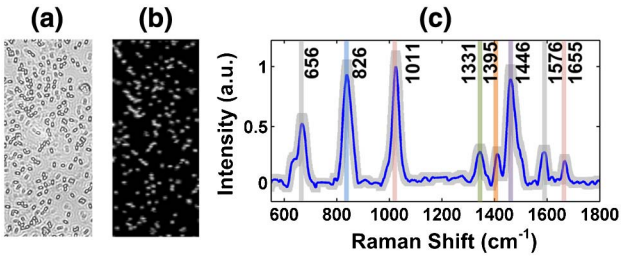

Fig. 4. Rapid identification and counting of bacterial spores using LSRM. (a) Bright-field image of more than 100 spores. (b) Map generated using CaDPA Raman peak. (c) Mean and standard deviation of Raman spectra of *Bacillus subtilis* spores.

spectra from all the spores with the solid line denoting the mean spectrum and the shaded area ±1 standard deviation. Strong Raman bands at 656 cm^{-1}, 826 cm^{-1}, 1011 cm^{-1}, 1395 cm^{-1}, 1445 cm^{-1}, and 1576 cm^{-1} are assigned to CaDPA and are in good agreement with previous studies [25,26]. Bands at 1655 cm^{-1} is assigned to protein amide I. The Raman image consisting of 151 spores was acquired within 1 h, or 2.5 spores/ min, which is already faster than one of the fastest results at 2 spores/ min [25]. LSRM throughput can be much higher with a sample with higher spore coverage. For example, an order of magnitude higher throughput can be easily achieved if the spatial coverage of bacteria is increased from the current value of 8%–80%.

5. Chemical Imaging of Colonial Microalgal Cell Using LSRM

Using Raman microscopy to study metabolites, lipids, and hydrocarbons in intact microalgae bioreactors has recently attracted significant interest due to the importance of understanding spatiotemporal molecular composition and the associated biosynthesis pathways for nutrition product and biofuels [8]. For example, hydrocarbon botryococcenes are hypothesized to experience multistep methylation as they migrate from the intracellular space to the extracellular environment [9]. However, such hypothetical pathway is still not well understood because of a lack of label-free molecular imaging technique. Existing mapping approaches are severely limited by slow mapping speed, low signal-to-noise ratio, and interference by strong background fluorescence [8,9], resulting in unsuccessful Raman mapping results [9]. We have applied LSRM to study the chemical distribution in a colonial microalgae, *Botryococcus braunii*, B race for the analysis of intra- and extracellular lipids and hydrocarbons. This green microalga produce triterpenes known as botryococcenes that can be converted into high-octane gasoline, kerosene, and diesel fuels. Botryococcenes have unique Raman bands near 1647 cm^{-1} to 1667 cm^{-1}, while common lipids such as saturated and unsaturated triglycerides, and hydrocarbons have Raman band at 1440 cm^{-1}. The chlorophyll map [Fig. 5(b)]

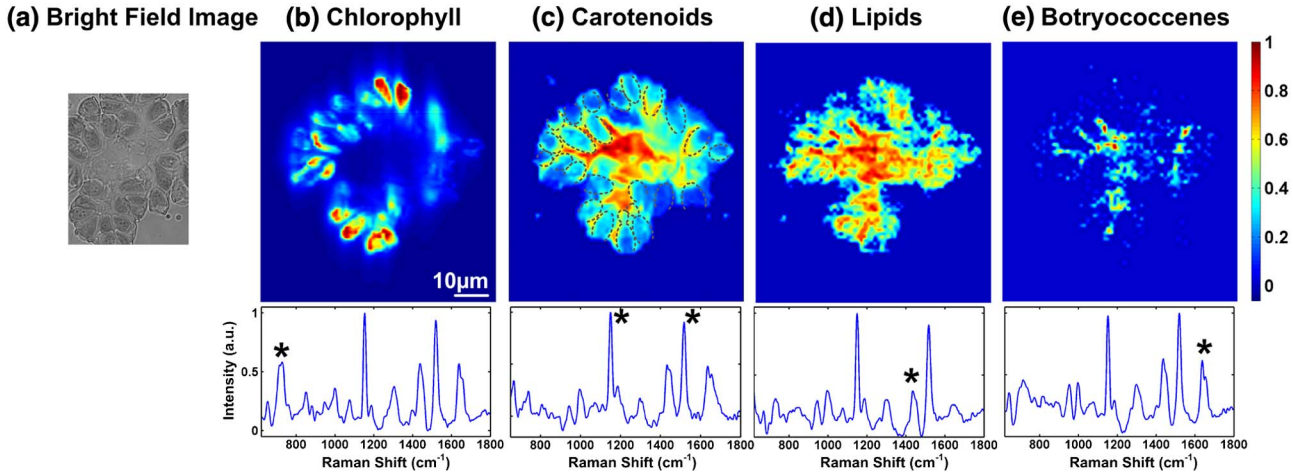

Fig. 5. Chemical imaging of colonial microalgae using LSRM. (a) Bright-field image; Raman maps generated for (b) chlorophyll, (c) carotenoids, (d) lipids, and (e) botryococcenes with representative Raman spectrum under each map.

generated from Raman band at 745 cm^{-1} and carotenoids map [Fig. 5(c)] generated from Raman band at 1520 cm^{-1} clearly showed the cell morphology. Representative cell boundaries were highlighted using dotted lines. Total lipids shown in Fig. 5(d) were found both inside the cell and in the extra-cellular matrix. Botryococcenes presented in Fig. 5(e) were primarily found in the extra-cellular matrix, which suggests a more advanced methylation stage of triterpene. The relative amounts of individual molecular constituents can be assessed semi-quantitatively using the color bar. The entire Raman data cube has been collected within 60 min *without* a pre-photobleaching step.

6. Conclusion

In conclusion, we have evaluated the performance of a high-throughput line-scan Raman microscope for chemical microscopy of cell population. We have presented a detailed system configuration and performed careful characterization for image uniformity and resolution. The overall image-acquisition time is significantly reduced by ~100 times compared to conventional Raman imaging methods but provides comparable spatial and spectral resolution. We have demonstrated the rapid-imaging capability of this instrument in test involving (1) the identification and counting of organic microparticles that appear identical in a bright-field image but differ in their chemical signature; (2) chemical imaging of bacterial spores; (3) chemical mapping of colonial microalgal cells. These results suggest that LSRM can be a highly versatile tool for studying cells at the population level without the need for labeling.

We thank Dr. M. Fujita for providing the bacteria samples and Drs. T. Devarenne and T. Weiss for the microalgae samples. We acknowledge funding from the National Science Foundation (NSF) CAREER Award (CBET-1151154), the National Aeronautics and Space Administration (NASA) Early Career Faculty Grant (NNX12AQ44G), the Gulf of Mexico Research Initiative (GoMRI-030), and the Cullen College of Engineering at the University of Houston.

References

1. G. J. Puppels, F. F. M. Demul, C. Otto, J. Greve, M. Robertnicoud, D. J. Arndtjovin, and T. M. Jovin, "Studying single living cells and chromosomes by confocal Raman microspectroscopy," Nature **347**, 301–303 (1990).
2. C. Matthaus, S. Boydston-White, M. Miljkovic, M. Romeo, and M. Diem, "Raman and infrared microspectral imaging of mitotic cells," Appl. Spectrosc. **60**, 1–8 (2006).
3. L. Hartsuiker, N. J. L. Zeijen, L. Terstappen, and C. Otto, "A comparison of breast cancer tumor cells with varying expression of the Her2/neu receptor by Raman microspectroscopic imaging," Analyst **135**, 3220–3226 (2010).
4. A. S. Haka, K. E. Shafer-Peltier, M. Fitzmaurice, J. Crowe, R. R. Dasari, and M. S. Feld, "Diagnosing breast cancer by using Raman spectroscopy," Proc. Natl. Acad. Sci. USA **102**, 12371–12376 (2005).
5. V. V. Pully, A. T. M. Lenferink, and C. Otto, "Time-lapse Raman imaging of single live lymphocytes," J. Raman Spectrosc. **42**, 167–173 (2011).
6. B. D. Beier, R. G. Quivey, and A. J. Berger, "Identification of different bacterial species in biofilms using confocal Raman microscopy," J. Biomed. Opt. **15**, 066001 (2010).
7. T. Chernenko, C. Matthaus, L. Milane, L. Quintero, M. Amiji, and M. Diem, "Label-free Raman spectral imaging of intracellular delivery and degradation of polymeric nanoparticle systems," Acs Nano **3**, 3552–3559 (2009).
8. Y. Y. Huang, C. M. Beal, W. W. Cai, R. S. Ruoff, and E. M. Terentjev, "Micro-Raman spectroscopy of algae: composition analysis and fluorescence background behavior," Biotechnol. Bioeng. **105**, 889–898 (2010).
9. T. L. Weiss, H. J. Chun, S. Okada, S. Vitha, A. Holzenburg, J. Laane, and T. P. Devarenne, "Raman Spectroscopy analysis of botryococcene hydrocarbons from the green microalga *Botryococcus braunii*," J. Biol. Chem. **285**, 32458–32466 (2010).
10. C. L. Evans, E. O. Potma, M. Puoris'haag, D. Cote, C. P. Lin, and X. S. Xie, "Chemical imaging of tissue *in vivo* with video-rate coherent anti-Stokes Raman scattering microscopy," Proc. Natl. Acad. Sci. USA **102**, 16807–16812 (2005).
11. C. W. Freudiger, W. Min, B. G. Saar, S. Lu, G. R. Holtom, C. W. He, J. S. Tsai, J. X. Kang, and X. S. Xie, "Label-free biomedical imaging with high sensitivity by stimulated Raman scattering microscopy," Science **322**, 1857–1861 (2008).
12. J. Qi, P. Motwani, M. Gheewala, C. Brennan, J. C. Wolfe, and W.-C. Shih, "Surface-enhanced Raman spectroscopy with monolithic nanoporous gold disk substrates," Nanoscale **5**, 4105–4109 (2013).
13. B. R. Masters and A. A. Thaer, "Real-time scanning slit confocal microscopy of the *in vivo* human cornea," Appl. Opt. **33**, 695–701 (1994).
14. M. B. Sinclair, J. A. Timlin, D. M. Haaland, and M. Werner-Washburne, "Design, construction, characterization, and application of a hyperspectral microarray scanner," Appl. Opt. **43**, 2079–2088 (2004).
15. W. C. Shih, K. L. Bechtel, and M. S. Feld, "Constrained regularization: hybrid method for multivariate calibration," Anal. Chem. **79**, 234–239 (2007).
16. A. M. K. Enejder, T. G. Scecina, J. Oh, M. Hunter, W. C. Shih, S. Sasic, G. L. Horowitz, and M. S. Feld, "Raman spectroscopy for noninvasive glucose measurements," J. Biomed. Opt. **10**, 031114 (2005).
17. M. Okuno and H. Hamaguchi, "Multifocus confocal Raman microspectroscopy for fast multimode vibrational imaging of living cells," Opt. Lett. **35**, 4096–4098 (2010).
18. A. D. Gift, J. Y. Ma, K. S. Haber, B. L. McClain, and D. Ben-Amotz, "Near-infrared Raman imaging microscope based on fiber-bundle image compression," J. Raman Spectrosc. **30**, 757–765 (1999).
19. W. C. Shih, K. L. Bechtel, and M. S. Feld, "Intrinsic Raman spectroscopy for quantitative biological spectroscopy Part I: theory and simulations," Opt. Express **16**, 12726–12736 (2008).
20. K. Hamada, K. Fujita, N. I. Smith, M. Kobayashi, Y. Inouye, and S. Kawata, "Raman microscopy for dynamic molecular imaging of living cells," J. Biomed. Opt. **13**, 044027 (2008).
21. K. A. Christensen and M. D. Morris, "Hyperspectral Raman microscopic imaging using Powell lens line illumination," Appl. Spectrosc. **52**, 1145–1147 (1998).
22. J. Qi and W.-C. Shih, "Parallel Raman microspectroscopy using programmable multi-point illumination," Opt. Lett. **37**, 1289–1291 (2012).
23. J. Qi, J. Li, and W.-C. Shih, "High-speed hyperspectral Raman imaging for label-free compositional microanalysis," Biomed. Opt. Express **4**, 2376–2382 (2013).
24. S. Schlucker, M. D. Schaeberle, S. W. Huffman, and I. W. Levin, "Raman microspectroscopy: a comparison of point, line, and wide-field imaging methodologies," Analyt. Chem. **75**, 4312–4318 (2003).
25. S. Stockel, S. Meisel, R. Bohme, M. Elschner, P. Rosch, and J. Popp, "Effect of supplementary manganese on the sporulation of Bacillus endospores analysed by Raman spectroscopy," J. Raman Spectrosc. **40**, 1469–1477 (2009).
26. J. W. Chan, A. P. Esposito, C. E. Talley, C. W. Hollars, S. M. Lane, and T. Huser, "Reagentless identification of single bacterial spores in aqueous solution by confocal laser tweezers Raman spectroscopy," Anal. Chem. **76**, 599–603 (2004).